

(Extended Abstract) - Advanced Kalman Filter Carrier Tracking: Performance Assessment under Two Ionospheric Scintillation Models

Rodrigo de Lima Florindo¹

¹Aeronautics Institute of Technology (ITA), São José dos Campos, SP, Brazil.

1. Scope Contextualization

Ionospheric scintillation is a physical phenomenon that causes amplitude fades and phase fluctuations on transionospheric signals due to ionospheric irregularities that may occur in both low- and high-latitude [5] regions. This effect impacts GNSS signals [29], LEO satellite communications [22], and radar signals [2], among others.

Several studies have reported that ionospheric scintillation can significantly degrade the reliability of some life-critical services that depend on precise position, navigation, and timing (PNT) solutions, such as precise point positioning (PPP) [4], [11], [15] and real-time kinematics (RTK) [3], [9] algorithms. Furthermore, it may also have a strong negative impact on the quality of scientific remote sensing data, including GNSS reflectometry [8] and synthetic aperture radar images [2].

On the other hand, by monitoring and analyzing the signal distortions inherent to scintillating signals, it is possible to obtain meaningful information about the structure and underlying physical properties of the ionosphere. This information can, in turn, be used to anticipate natural disasters—such as volcanic activity [24] and earthquakes [20]—or even to monitor the potential use of nuclear defense weapons [23].

Hence, there is a growing need for the development of GNSS receivers that are both robust and capable of providing meaningful data regarding scintillation effects. Considering the nature of ionospheric scintillation, one may foresee that the most susceptible part of the GNSS signal processing chain is the tracking module—particularly the carrier phase tracking. Over the past decades, the scientific community has dedicated significant effort to characterizing the effects of scintillation on carrier phase tracking algorithms, with the aim of establishing a framework that researchers can use to develop new, more reliable tracking methods under such conditions [18].

[1] analyzed several recorded scintillation events to determine optimal configurations for the Costas phase-locked loop (PLL) used in carrier phase tracking algorithms, allowing these systems to better handle scintillating signals. They also laid the foundation for a statistical model to help researchers develop more robust tracking loops. In this work, the authors pointed out that using Kalman filter (KF)-based PLLs could lead to more robust solutions. Later, this statistical model—referred to in many works as the Cornell Scintillation Model (CSM)—was further developed in [29], [28]. This model generates a time series of the diffractive effects of equatorial ionospheric scintillation using filtered Gaussian noise, and it has since gained popularity among GNSS researchers due to its simplicity and computational efficiency.

Given the Gaussian nature of the scintillation time series generated by the CSM, [6], [25] have initially proposed to augment the state space model of a KF based PLL with an autoregressive model (KF-AR), and also to use of an extended KF (EKF) to also track the amplitude fades caused by scintillation. In [13], the usage of Adaptive KF (AKF) under scintillation was introduced and it was further discussed in [7]. Subsequently, this approach was further developed for any order of AR models in [13] and a multi-frequency KF and EKF augmented with a multivariate AR (KF-MAR) model system was proposed in [10].

Later, [19] and [21] comprehensively evaluated the benefits of augmenting the KF state-space with AR models under scintillation conditions. In these studies, a robust variant of the KF-AR model—known as the Adaptive Hard-Limited KF-AR (AHL-KF-AR)—was proposed. This approach applies a constraint to the adaptive module

of the KF so that whenever the amplitude fades beyond a certain threshold, the diagonal values of the measurement covariance matrix become extremely large, thereby reducing the occurrence of cycle slips.

Another aspect that has been thoroughly discussed in this context is online AR model parameter estimation. Initially, [14] proposed using block and sliding windows to adaptively estimate the model parameters in real time. Then, [27] developed a dual KF topology capable of recursively estimating both the AR model parameters and the phase estimates using two separate Kalman filters that mutually benefit one another. More recently, [30] proposed employing a radial basis function (RBF) network to estimate the scintillation phase and amplitude states in conjunction with a Kalman filter that tracks the line-of-sight (LOS) dynamics.

It is noteworthy, however, that all the previous works were developed and validated using scintillation effects generated either by the CSM or by recorded and post-processed real data from scintillation events. The reliability of the CSM in representing real scintillation events was recently contested in a new study, which proposed a compact GNSS scintillation model (referred to in this work as the TPPSM) based on a two-component power law phase screen model [12]. Additionally, recent works have argued that important scintillation features of the received signal may be lost during the phase detrending process [16]. Consequently, it is necessary to evaluate the advanced tracking modules proposed over the past decades to understand their behavior under a state-of-the-art (SoA) scintillation model.

The purpose of this work is to discuss and compare the behavior of the most prominent KF-AR topologies—considering only offline AR parameter estimation—under severe ionospheric scintillation events simulated by both the CSM and the newly developed TPPSM.

2. Preliminary Results and Discussions

The behavior of the following topologies is evaluated in this section:

- **KF-Std:** Standard KF PLL (Output of interest: $\hat{\phi}[k|k-1]$)
- **AKF-Std:** Adaptive Standard KF PLL (Output of interest: $\hat{\phi}[k|k-1]$)
- **AHL-KF-Std:** Adaptive Hard-Limited Standard KF PLL (Output of interest: $\hat{\phi}[k|k-1]$)
- **KF-AR:** Autoregressive KF PLL (Outputs of interest: $\hat{\phi}_{\text{LOS}}[k|k-1], \hat{\phi}_s[k|k-1]$)
- **AKF-AR:** Adaptive Autoregressive KF PLL (Outputs of interest: $\hat{\phi}_{\text{LOS}}[k|k-1], \hat{\phi}_s[k|k-1]$)
- **AHL-KF-AR:** Adaptive Hard-Limited Autoregressive KF PLL (Outputs of interest: $\hat{\phi}_{\text{LOS}}[k|k-1], \hat{\phi}_s[k|k-1]$)

The following parameters were used to obtain the results shown in this section:

1. General parameters

- Line-of-sight dynamics profile: Initial phase equal to 0 radians; 1000 Hz of Doppler shift; and 0.94 Hz/s of Doppler drift
- Baseline carrier-to-noise ratio $\overline{C/N_0} = 42$ [dB-Hz]
- Simulation settling time: 50 seconds (This is adopted to guarantee that the topologies estimates have converged before dealing with the scintillation event.)
- Sampling interval: 10 ms
- AR model order: 5

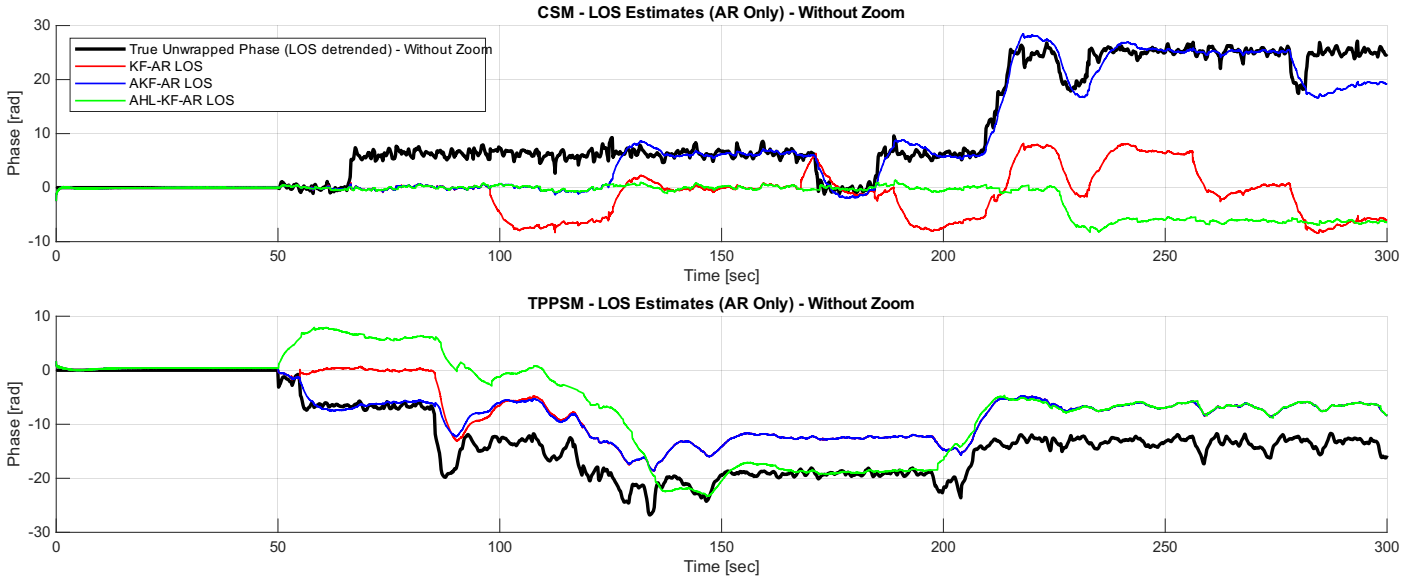


Figure 1. Estimated line-of-sight phase time series $\hat{\phi}_{LOS}[k|k-1] \forall k$ for each of the considered KF-based PLL topologies.

- Simulation time length of the data used to estimate the AR model parameters: 1500 seconds;
- Process noise variance: For the time series examples shown in figs. 1 to 3, it was chosen as $\sigma_3^2 = 2.6 * 10^{-6}$, which represents the highest value for a static receiver [26, Example 1].
- Hard-limited threshold: 38dB-Hz.

2. Ionospheric scintillation models input parameters

- Cornell Scintillation Model
 - Scintillation Intensity: $S_4 = 0.8$;
 - Decorrelation time: $\tau_0 = 0.5$;
- Compact GNSS Scintillation Model (TPPSM)
 - Universal Turbulance Strength: $U = 2$
 - normalized wavenumber spectral break: $\mu_0 = 0.5$
 - Low-frequency spectral index: $p_1 = 2.45$
 - High-frequency spectral index: $p_2 = 3.7$
 - Receiver position (latitude [rad], longitude [rad] and height [m]): $\{0.3876, 1.9942, 59.6780\}$;
 - Date and time (Year, Month, Day, Hour, Minutes, Seconds): $\{2014, 01, 02, 10, 00, 00\}$;
 - Satellite PRN: 18;
 - Simulation time length: 300 s;
 - Eastward drift velocity: 125 m/s.

It is possible to observe examples of the behavior of the state outputs of the studied topologies when submitted through severe scintillation events generated by the CSM and the TPPSM in figures figs. 1 to 6. It is noteworthy that the hard-limited threshold was heuristically chosen to enable the AHL-KF-AR topology to avoid the occurrence of cycle-slips for the CSM algorithm.

To further analyze the behavior of each topology, figs. 7 to 18 presents heatmaps that shows the most common values of RMSE. In these plots, the rows represent the bins of histograms for the RMSE values corresponding to the LOS, scintillation, and joint phase, computed from 500 Monte Carlo runs. The columns show different values of the process noise variance, which were sampled in 50 logarithmically spaced steps within the interval $\sigma_3^2 \in [10^{-4}, 10^{-8}]$, using 50 bins for each histogram. Additionally, a white solid line was plotted together with the heatmap, which denotes the mean values of the obtained RMSE—for each process noise variance—and two white dashed lines denotes the 5% and 95% confidence bounds of the obtained RMSE values.

The values of the RMSEs for the LOS, scintillation and joint phase estimates of the KF PLLs augmented with AR models were computed as shown in equations eqs. (1) to (3)

$$\text{RMSE}_{\text{scint}} = \sqrt{\frac{1}{K} \sum_{k=1}^K (\hat{\phi}_s[k|k-1] - \text{WrapToPi}(\phi_s[k]))^2} \quad (1)$$

In the standard KF PLLs, where there is only a single joint phase that captures the LOS dynamics and the scintillation phase together, we computed its RMSE as it is shown on equation eq. (4). It is important to comment here that the usage of a wrapping function to compute the RMSE is common, given that it prevents undetected cycle-slips to increase the RMSE without bounds [10], [13], [27].

2.1. LOS phase estimate behavior comparison

Figures figs. 7 and 8 depict the behavior of the estimated LOS phase for the KF-AR and AKF-AR topologies. It is evident that both topologies suffer significant performance degradation when subjected to the CSM and TPPSM scintillation models. As shown in figs. 1 and 6, the LOS phase estimates require a settling period— inversely proportional to the chosen process noise variance—to converge following a cycle-slip occurrence. The very high RMSE values further indicate that the precision of the LOS phase estimates was severely compromised by multiple cycle slips.

On the other hand, Figure 8 shows that the LOS phase estimates provided by the AHL-KF-AR topology exhibit considerably higher precision under the CSM model. Examination of figs. 1 and 6 reveals that this topology produced more robust phase estimates, with only a single cycle slip observed, whereas the other topologies experienced numerous cycle-slip events. Moreover, the reduction in RMSE appears to be related to the absence of a prolonged settling phase after a cycle slip. However, despite its promising performance under the CSM model, the AHL-KF-AR topology could not maintain its robustness when subjected to the TPPSM. This suggests that, under realistic severe ionospheric scintillation scenarios, even advanced KF PLLs—presumably designed to be robust to scintillation—struggle to avoid cycle slips or, at the very least, to prevent degradation in LOS phase estimates.

2.2. Scintillation phase estimate behavior comparison

Similarly to the LOS phase estimates, Figures figs. 10 and 11 indicate that the KF-AR and AKF-AR topologies were unable to provide robust

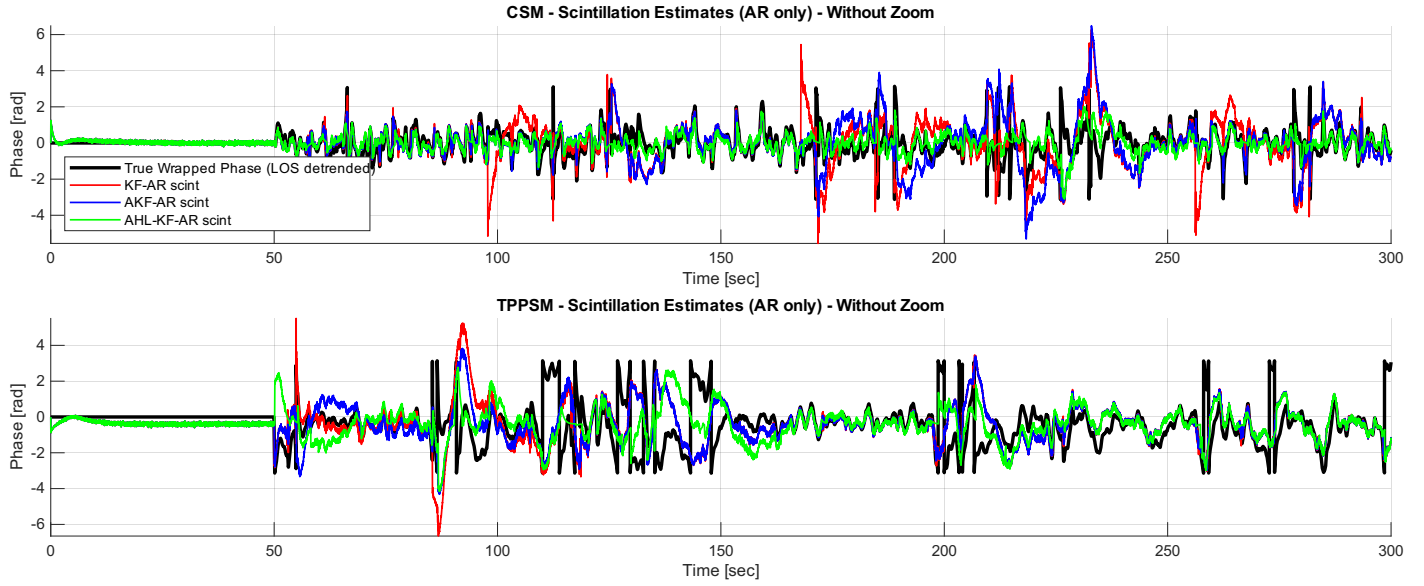


Figure 2. Estimated scintillation phase time series $\hat{\phi}_s[k|k-1] \forall k$ (for KF models augmented with AR models, we have $\hat{\phi}[k|k-1] = \hat{\phi}_{LOS}[k|k-1] + \hat{\phi}_s[k|k-1]$) for each of the considered KF-based PLL topologies.

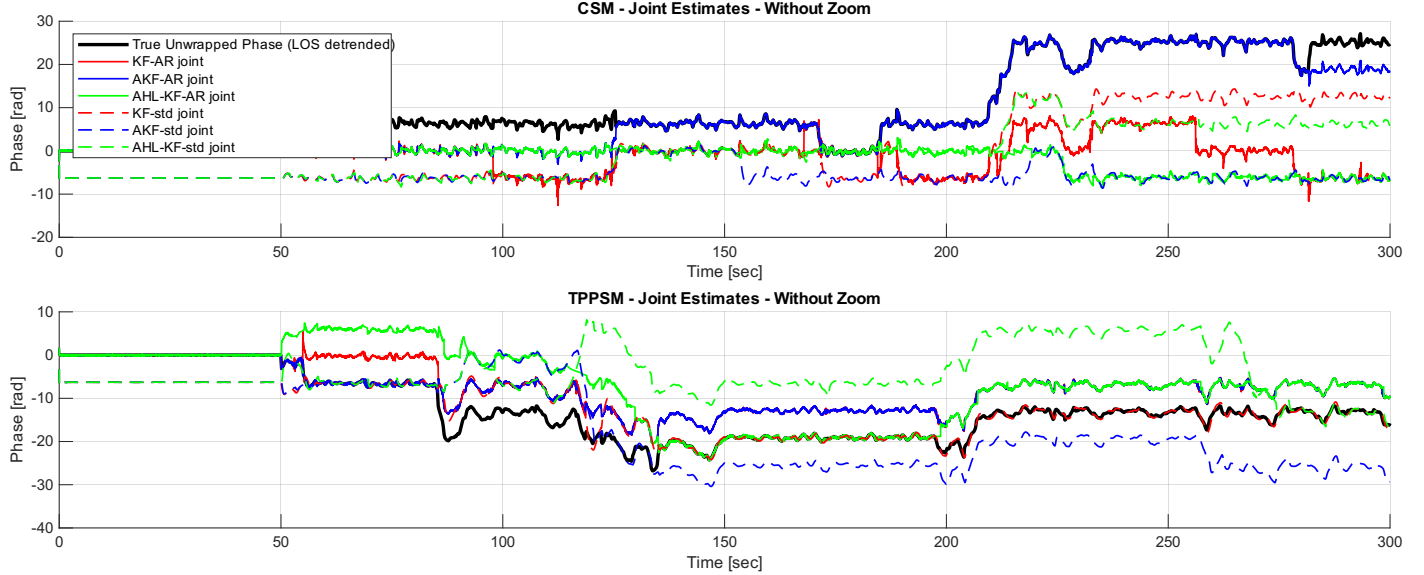


Figure 3. Estimated joint phase time series $\hat{\phi}_{LOS}[k|k-1] \forall k$ (for KF models augmented with AR models, we have $\hat{\phi}[k|k-1] = \hat{\phi}_{LOS}[k|k-1] + \hat{\phi}_s[k|k-1]$) for each of the considered KF-based PLL topologies.

scintillation phase estimates under severe scintillation conditions for both the CSM and TPPSM models. Although the AHL-KF-AR topology achieved considerably higher precision for scintillation phase estimates under the CSM model, it could not operate properly under the TPPSM. Additionally, the AHL-KF-AR topology attempts to mitigate cycle slips by momentarily increasing the measurement noise covariance when the received signal's carrier-to-noise ratio drops below a configured threshold [21]. This behavior is further evidenced in Figure 5, which shows that whenever a cycle slip is likely to occur, the scintillation phase estimates become less responsive. In other words, with higher measurement uncertainty, the KF relies more heavily on the process dynamics.

Notably, there appears to be a tendency for the scintillation phase RMSE to decrease as the process noise variance increases, suggesting that the scintillation phase estimates become less responsive under these conditions. Analysis of the measurement model reveals that the KF-AR topologies generate a single phase estimate—used to derive the phase error relative to the received signal—by summing the LOS and scintillation phase state estimates. Therefore, when the LOS

process noise variance increases, the LOS phase estimates contribute more to the joint phase, causing the scintillation phase estimates to become less responsive and to fluctuate around zero. Furthermore, as observed in figs. 2 and 5, each time a cycle slip occurs the scintillation phase becomes unstable and requires some time to converge toward the true phase. In addition, smaller process noise variance values are expected to prolong the transient phase following a cycle slip, given the direct proportionality between the process noise variance and the equivalent loop bandwidth [17, Section 6.4.1.1]. Consequently, the occurrence of cycle slips introduces a distortion in the RMSE due to the transient phase, causing the scintillation phase estimates to momentarily diverge from the true phase.

2.3. Joint phase estimate behavior comparison

We can infer from figures figs. 13, 17 and 18, and also considering figs. 3 and 6 that the phase estimates of the standard KF topologies presented a very slow responsiveness, which degraded the RMSE. Additionally, despite the increase of the process noise variance, the RMSE did not decreased significantly. By comparing now the afore-

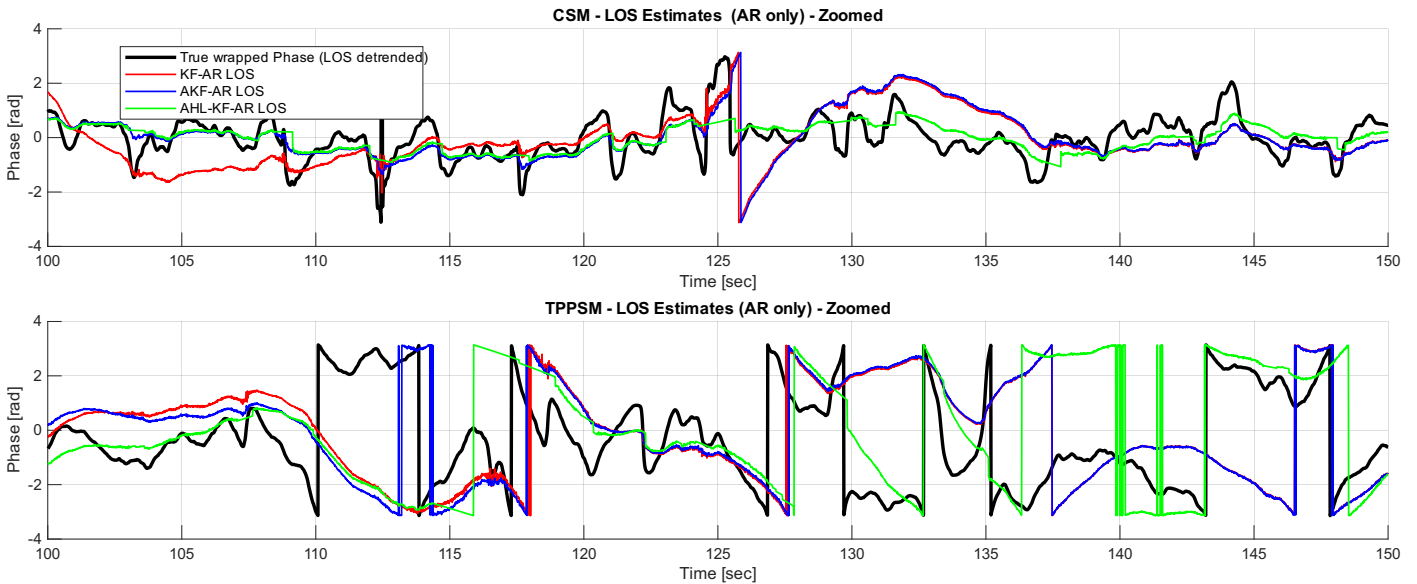


Figure 4. Zoomed Estimated line-of-sight phase time series $\hat{\phi}_{LOS}[k|k-1] \forall k$ for each of the considered KF-based PLL topologies.

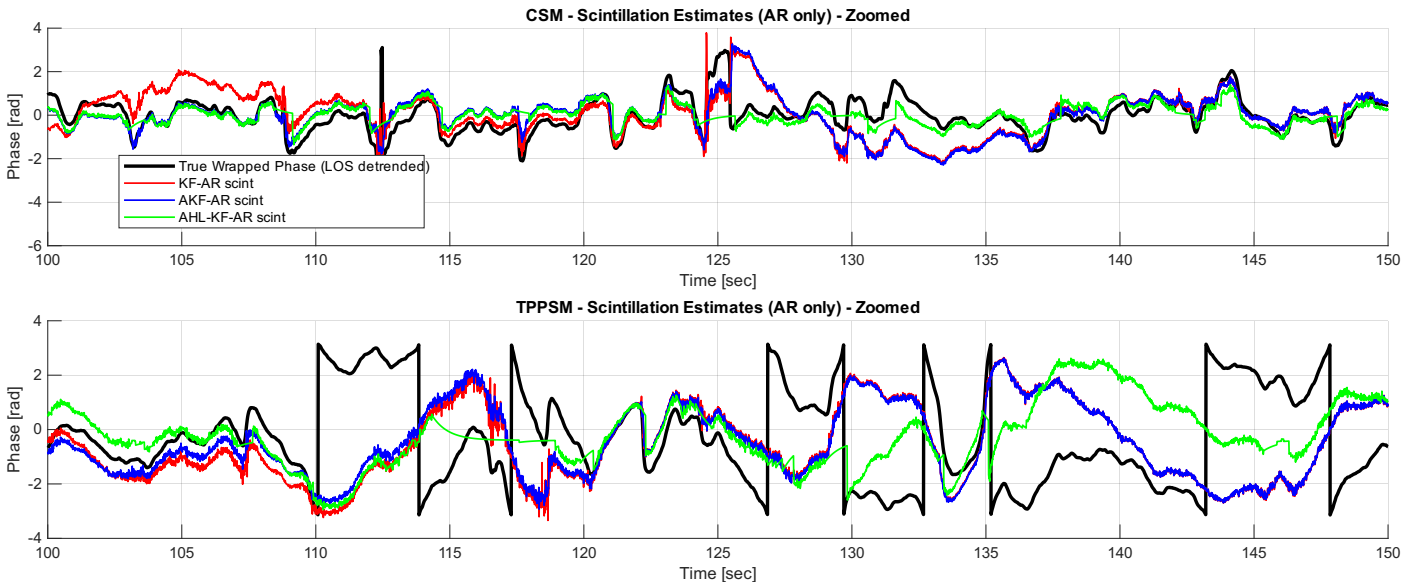


Figure 5. Zoomed Estimated scintillation phase time series $\hat{\phi}_s[k|k-1] \forall k$ (for KF models augmented with AR models, we have $\hat{\phi}[k|k-1] = \hat{\phi}_{LOS}[k|k-1] + \hat{\phi}_s[k|k-1]$) for each of the considered KF-based PLL topologies.

mentioned set of figures with the figs. 16 to 18, we can observe that the augmented KF-AR topologies showed lesser RMSE values than the standard KF ones, for both the CSM and the TPPSM scenarios. With that, we can infer that the augmentation with a AR model also affects the equivalent loop bandwidth, as it well discussed in [17, Section 5.9.1].

Moreover, we can also observe that the joint phase estimates of the AHL-KF-AR topology presented the poorest RMSE among the AR topologies, under both CSM and TPPSM. By analyzing figure 6, we can infer that the increased RMSE values might be related to the cases where the estimated carrier-to-noise ratio have dropped below the configured threshold and then the estimated phase estimates freezes.

■ References

- [1] T. Humphreys, M. Psiaki, and P. Kintner, “Gps carrier tracking loop performance in the presence of ionospheric scintillations”, vol. 2005, Jan. 2005.
- [2] C. S. Carrano, K. M. Groves, and R. G. Caton, “Simulating the impacts of ionospheric scintillation on l band sar image formation”, *Radio Science*, vol. 47, no. 4, 2012. DOI: <https://doi.org/10.1029/2011RS004956>. eprint: <https://agupubs.onlinelibrary.wiley.com/doi/pdf/10.1029/2011RS004956>. [Online]. Available: <https://agupubs.onlinelibrary.wiley.com/doi/abs/10.1029/2011RS004956>.
- [3] K. S. Jacobsen and S. Schäfer, “Observed effects of a geomagnetic storm on an rtk positioning network at high latitudes”, *Journal of Space Weather and Space Climate*, vol. 2, 2012, ISSN: 21157251. DOI: [10.1051/swsc/2012013](https://doi.org/10.1051/swsc/2012013).
- [4] X. Zhang, F. Guo, and P. Zhou, “Improved precise point positioning in the presence of ionospheric scintillation”, *GPS Solutions*, vol. 18, pp. 51–60, 1 Jan. 2014, ISSN: 15211886. DOI: [10.1007/s10291-012-0309-1](https://doi.org/10.1007/s10291-012-0309-1).
- [5] Y. Jiao and Y. T. Morton, “Comparison of the effect of high-latitude and equatorial ionospheric scintillation on gps signals during the maximum of solar cycle 24”, *Radio Science*,

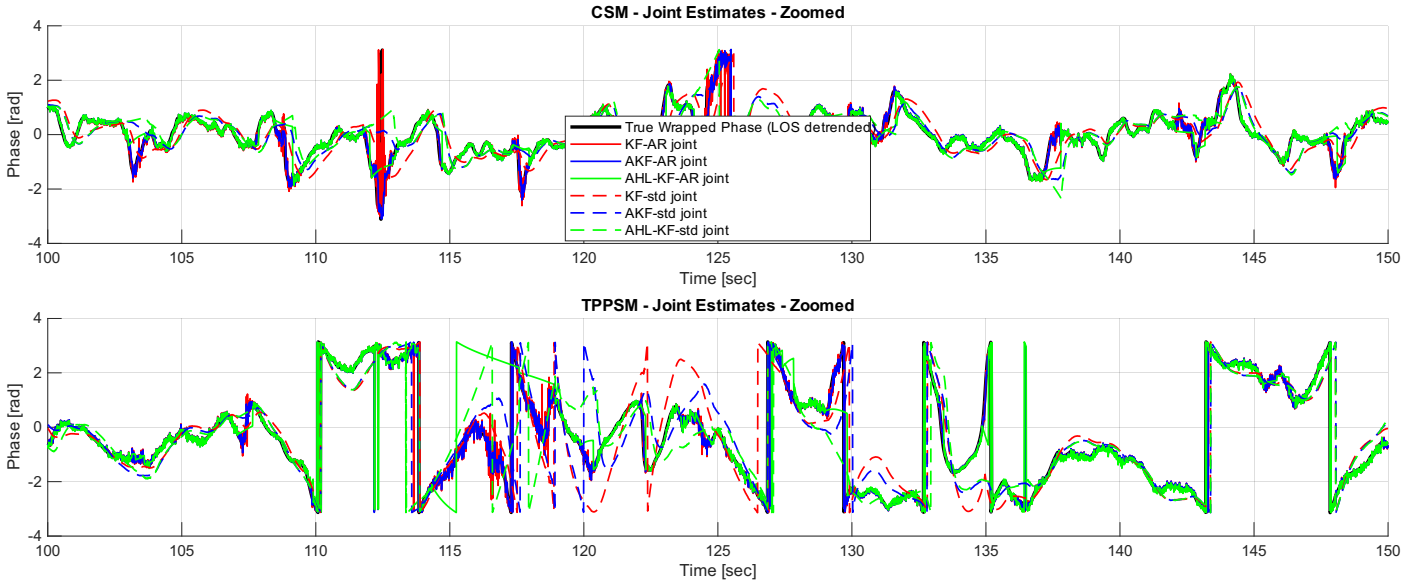


Figure 6. Zoomed Estimated joint phase time series $\hat{\phi}_{LOS}[k|k-1] \forall k$ (for KF models augmented with AR models, we have $\hat{\phi}[k|k-1] = \hat{\phi}_{LOS}[k|k-1] + \hat{\phi}_s[k|k-1]$) for each of the considered KF-based PLL topologies.

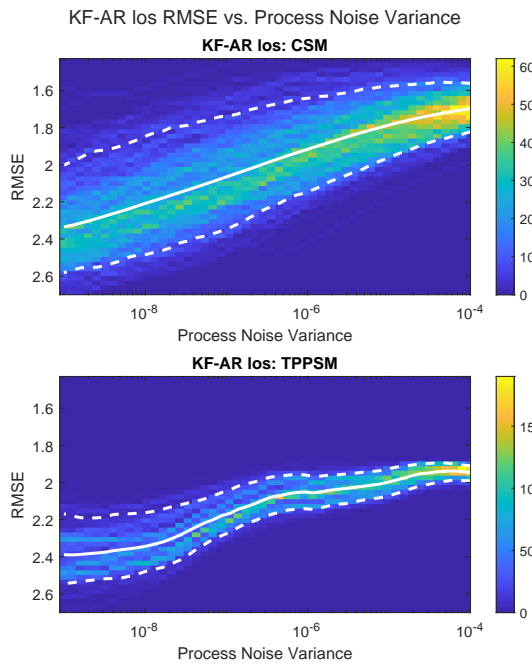


Figure 7. test

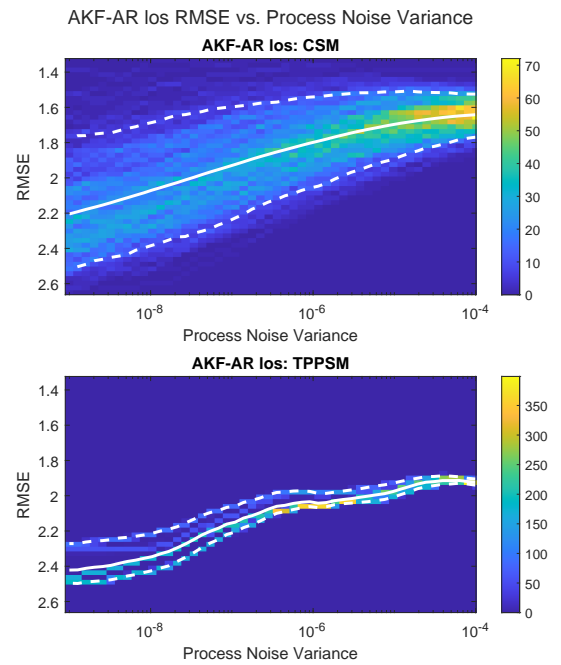


Figure 8. test

$$RMSE_{LOS} = \sqrt{\frac{1}{K} \sum_{k=1}^K (\text{WrapToPi}(\hat{\phi}_{LOS}[k|k-1]) - \text{WrapToPi}(\phi_{LOS}[k]))^2} \quad (2)$$

$$RMSE_{\text{joint}} = \sqrt{\frac{1}{K} \sum_{k=1}^K (\text{WrapToPi}(\hat{\phi}_{LOS}[k|k-1] + \hat{\phi}_s[k|k-1]) - \text{WrapToPi}(\phi_{LOS}[k]))^2} \quad (3)$$

$$RMSE_{\text{joint}}^* = \sqrt{\frac{1}{K} \sum_{k=1}^K (\text{WrapToPi}(\hat{\phi}[k|k-1]) - \text{WrapToPi}(\phi_{LOS}[k]))^2} \quad (4)$$

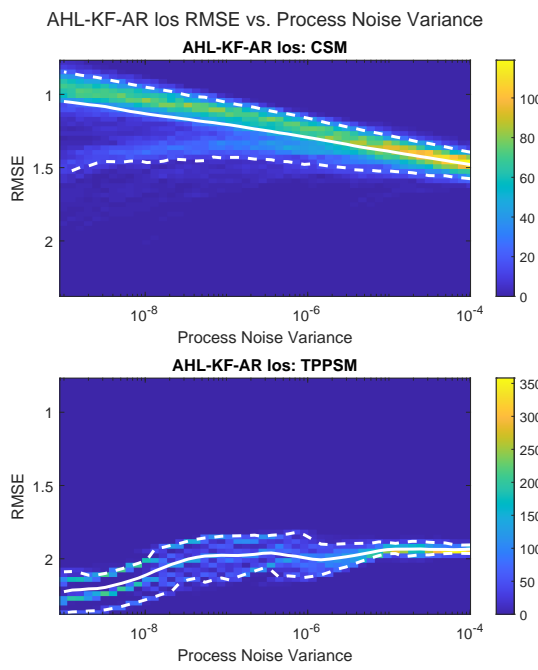


Figure 9. test

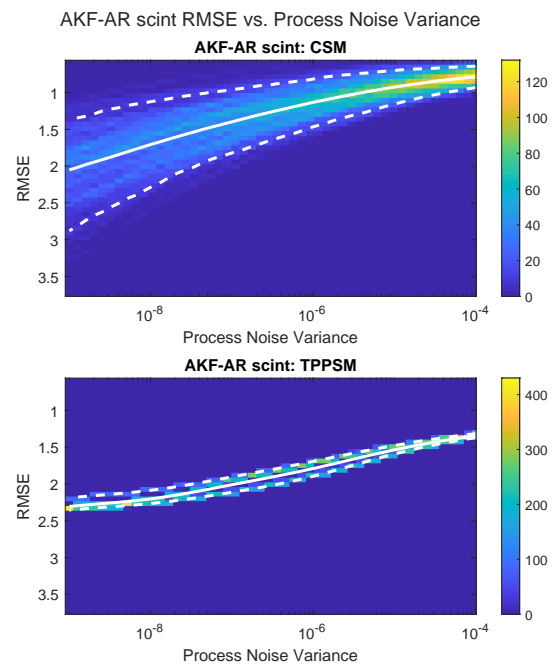


Figure 11. test

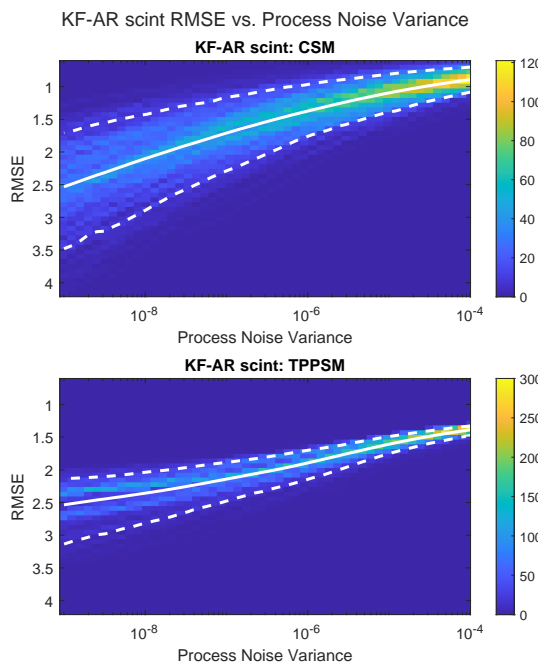


Figure 10. test

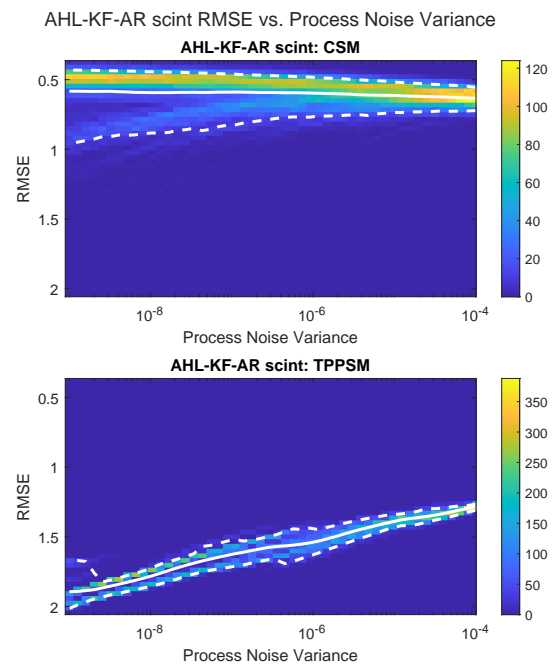
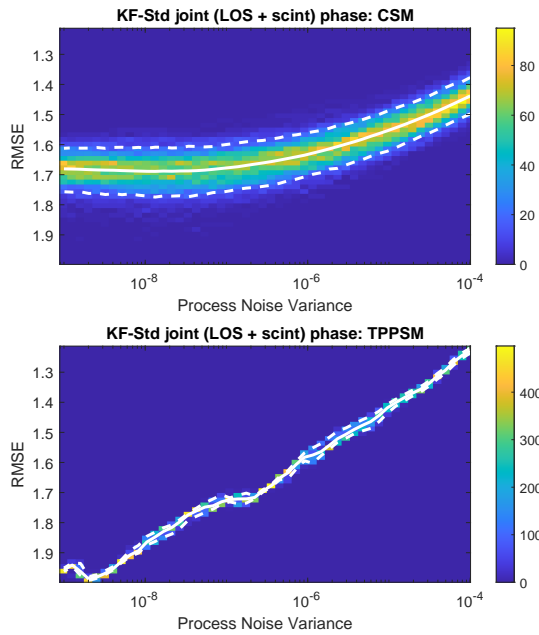
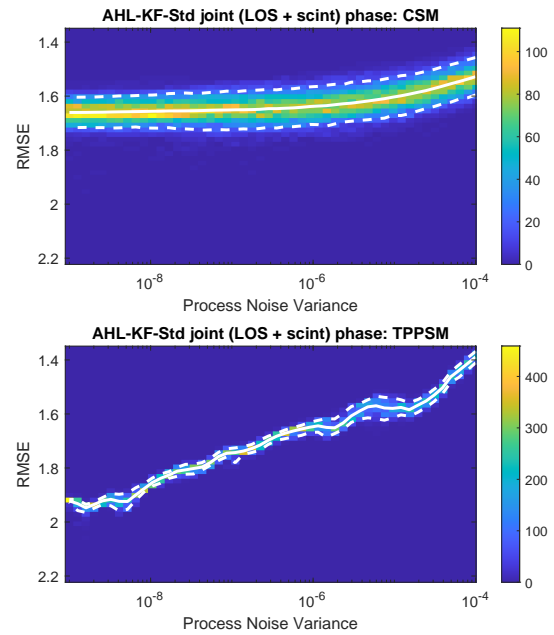


Figure 12. test

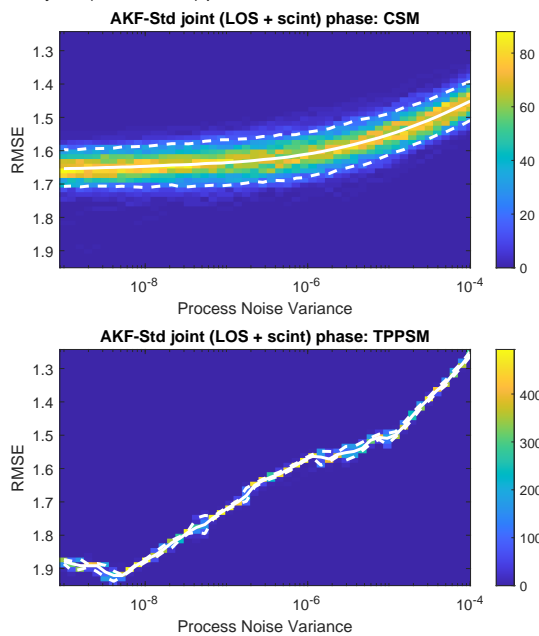
-Std joint (LOS + scint) phase RMSE vs. Process Noise Variance

**Figure 13.** test

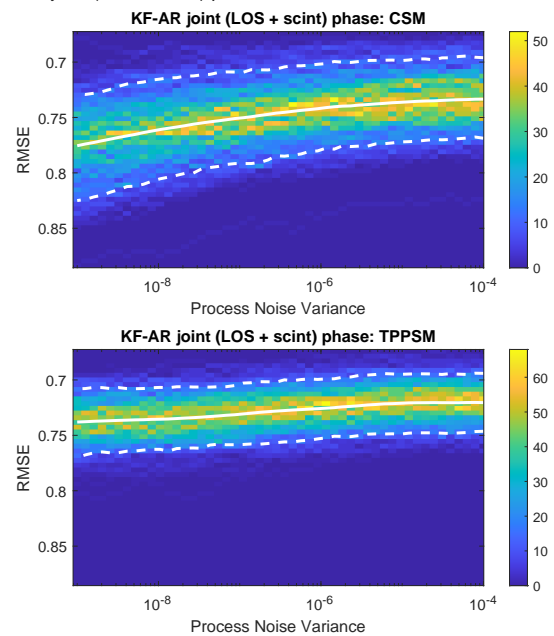
<-Std joint (LOS + scint) phase RMSE vs. Process Noise Variance

**Figure 15.** test

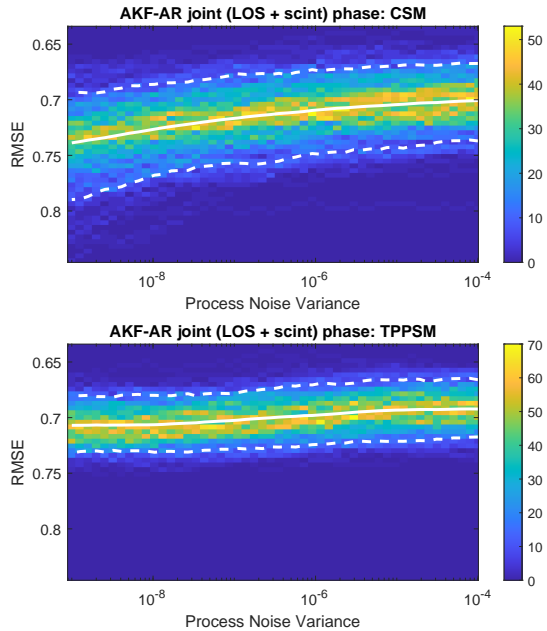
-Std joint (LOS + scint) phase RMSE vs. Process Noise Variance

**Figure 14.** test

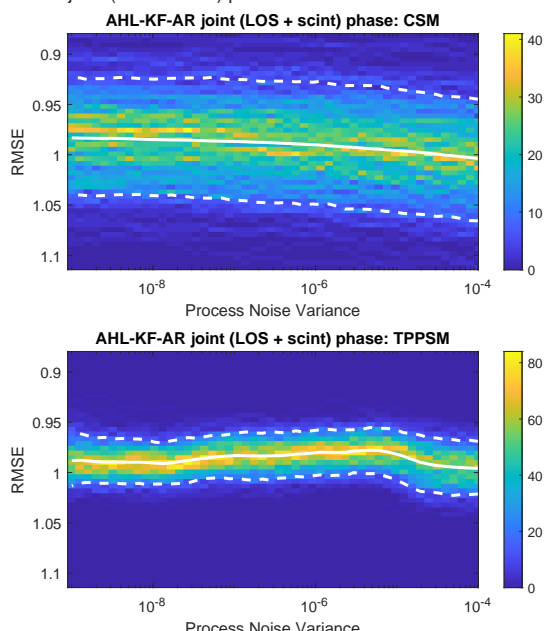
<-AR joint (LOS + scint) phase RMSE vs. Process Noise Variance

**Figure 16.** test

KF-AR joint (LOS + scint) phase RMSE vs. Process Noise Variance

**Figure 17. test**

-KF-AR joint (LOS + scint) phase RMSE vs. Process Noise Variance

**Figure 18. test**

vol. 50, no. 9, pp. 886–903, 2015. doi: <https://doi.org/10.1002/2015RS005719>. eprint: <https://agupubs.onlinelibrary.wiley.com/doi/pdf/10.1002/2015RS005719>. [Online]. Available: <https://agupubs.onlinelibrary.wiley.com/doi/abs/10.1002/2015RS005719>.

- [6] J. Vilà-Valls, P. Closas, and C. Fernández-Prades, “Advanced kf-based methods for gnss carrier tracking and ionospheric scintillation mitigation”, in *2015 IEEE Aerospace Conference*, 2015, pp. 1–10. doi: [10.1109/AERO.2015.7118930](https://doi.org/10.1109/AERO.2015.7118930).
- [7] J. Vilà-Valls, P. Closas, C. Fernández-Prades, J. A. López-Salcedo, and G. Seco-Granados, “Adaptive gnss carrier tracking under ionospheric scintillation: Estimation vs. mitigation”, *IEEE Communications Letters*, vol. 19, no. 6, pp. 961–964, 2015. doi: [10.1109/LCOMM.2015.2415789](https://doi.org/10.1109/LCOMM.2015.2415789).
- [8] A. Camps, H. Park, G. Foti, and C. Gommenginger, “Ionospheric effects in gnss-reflectometry from space”, *IEEE Journal of Selected Topics in Applied Earth Observations and Remote Sensing*, vol. 9, no. 12, pp. 5851–5861, 2016. doi: [10.1109/JSTARS.2016.2612542](https://doi.org/10.1109/JSTARS.2016.2612542).
- [9] K. S. Jacobsen and Y. L. Andalsvik, “Overview of the 2015 St. Patrick’s day storm and its consequences for RTK and PPP positioning in norway”, *Journal of Space Weather and Space Climate*, vol. 6, 2016, ISSN: 21157251. doi: [10.1051/swsc/2016004](https://doi.org/10.1051/swsc/2016004).
- [10] Vilà-Valls, Jordi, Closas, Pau, and Curran, James T., “Multi-frequency gnss robust carrier tracking for ionospheric scintillation mitigation”, *J. Space Weather Space Clim.*, vol. 7, A26, 2017. doi: [10.1051/swsc/2017020](https://doi.org/10.1051/swsc/2017020). [Online]. Available: <https://doi.org/10.1051/swsc/2017020>.
- [11] X. Luo, S. Gu, Y. Lou, C. Xiong, B. Chen, and X. Jin, “Assessing the performance of GPS precise point positioning under different geomagnetic storm conditions during solar cycle 24”, *Sensors (Switzerland)*, vol. 18, 6 Jun. 2018, ISSN: 14248220. doi: [10.3390/s18061784](https://doi.org/10.3390/s18061784).
- [12] C. Rino, B. Breitsch, Y. Morton, Y. Jiao, D. Xu, and C. Carrano, “A compact multi-frequency GNSS scintillation model”, *NAVIGATION*, vol. 65, no. 4, pp. 563–569, 2018, ISSN: 2161-4296. doi: [10.1002/navi.263](https://doi.org/10.1002/navi.263). Accessed: 2024-08-02. [Online]. Available: <https://onlinelibrary.wiley.com/doi/abs/10.1002/navi.263>.
- [13] J. Vilà-Valls, P. Closas, C. Fernández-Prades, and J. T. Curran, “On the mitigation of ionospheric scintillation in advanced gnss receivers”, *IEEE Transactions on Aerospace and Electronic Systems*, vol. 54, no. 4, pp. 1692–1708, 2018. doi: [10.1109/TAES.2018.2798480](https://doi.org/10.1109/TAES.2018.2798480).
- [14] J. Vilà-Valls, C. Fernández-Prades, J. Arribas, J. T. Curran, and P. Closas, “On-line model learning for adaptive gnss ionospheric scintillation estimation and mitigation”, in *2018 IEEE/ION Position, Location and Navigation Symposium (PLANS)*, 2018, pp. 1167–1172. doi: [10.1109/PLANS.2018.8373501](https://doi.org/10.1109/PLANS.2018.8373501).
- [15] B. C. Vani et al., “A novel approach to improve GNSS precise point positioning during strong ionospheric scintillation: Theory and demonstration”, *IEEE Transactions on Vehicular Technology*, vol. 68, pp. 4391–4403, 5 May 2019, ISSN: 19399359. doi: [10.1109/TVT.2019.2903988](https://doi.org/10.1109/TVT.2019.2903988).
- [16] H. Ghobadi et al., “Disentangling ionospheric refraction and diffraction effects in gnss raw phase through fast iterative filtering technique”, *GPS Solutions*, vol. 24, Jun. 2020. doi: [10.1007/s10291-020-01001-1](https://doi.org/10.1007/s10291-020-01001-1).

- [17] S. Locubiche-Serra, "Robust carrier tracking techniques for gnss receivers affected by ionospheric scintillation", Doctoral thesis. Directors: José Antonio López Salcedo and Gonzalo Seco Granados. 1 recurs en línia (202 pàgines). ISBN 9788449089411., Ph.D. dissertation, Universitat Autònoma de Barcelona, 2020. Accessed: Feb. 27, 2025. [Online]. Available: <https://ddd.uab.cat/record/235075>.
- [18] J. Vilà-Valls, N. Linty, P. Closas, F. Dovis, and J. T. Curran, "Survey on signal processing for GNSS under ionospheric scintillation: Detection, monitoring, and mitigation", *NAVIGATION: Journal of the Institute of Navigation*, vol. 67, no. 3, pp. 511–535, 2020, ISSN: 0028-1522.
- [19] S. Locubiche-Serra, G. Seco-Granados, and J. A. López-Salcedo, "Performance limits and benefits of adaptive autoregressive kalman filters for gnss scintillation-robust carrier tracking", in *2021 International Conference on Localization and GNSS (ICL-GNSS)*, 2021, pp. 1–6. DOI: [10.1109/ICL-GNSS51451.2021.9452297](https://doi.org/10.1109/ICL-GNSS51451.2021.9452297).
- [20] Y. He, X. Zhao, D. Yang, Y. Wu, and Q. Li, "A study to investigate the relationship between ionospheric disturbance and seismic activity based on swarm satellite data", *Physics of the Earth and Planetary Interiors*, vol. 323, p. 106 826, 2022, ISSN: 0031-9201. DOI: <https://doi.org/10.1016/j.pepi.2021.106826>. [Online]. Available: <https://www.sciencedirect.com/science/article/pii/S0031920121001849>.
- [21] S. Locubiche-Serra, G. Seco-Granados, and J. A. López-Salcedo, "Performance assessment of a low-complexity autoregressive kalman filter for gnss carrier tracking using real scintillation time series", *GPS Solutions*, vol. 26, Jan. 2022. DOI: [10.1007/s10291-021-01193-0](https://doi.org/10.1007/s10291-021-01193-0).
- [22] Y. Morton, N. Xu, and Y. Jiao, "Ionospheric scintillation effects on signals transmitted from leo satellites", Oct. 2022, pp. 2980–2988. DOI: [10.33012/2022.18341](https://doi.org/10.33012/2022.18341).
- [23] B. A. Wilson, D. A. Hooper, A. Miloshevsky, W. P. Grice, and N. A. Peters, "Effects of a nuclear-disturbed environment on electromagnetic wave propagation through the atmosphere", *Opt. Express*, vol. 31, no. 3, pp. 3881–3896, Jan. 2023. DOI: [10.1364/OE.475466](https://doi.org/10.1364/OE.475466). [Online]. Available: <https://opg.optica.org/oe/abstract.cfm?URI=oe-31-3-3881>.
- [24] X. Chen, R. Zhang, X. Kong, Z. Liang, L. Su, and C. Wang, "Impact of tonga volcanic eruption on the ionosphere based on ground-based gnss and cosmic occultation data", *Advances in Space Research*, vol. 75, no. 1, pp. 1066–1076, 2025, ISSN: 0273-1177. DOI: <https://doi.org/10.1016/j.asr.2024.10.061>. [Online]. Available: <https://www.sciencedirect.com/science/article/pii/S0273117724010937>.
- [25] J. Vilà-Valls, J. López-Salcedo, and G. Seco-Granados. "An interactive multiple model approach for robust GNSS carrier phase tracking under scintillation conditions | IEEE Conference Publication | IEEE Xplore", Accessed: 2024-02-13. [Online]. Available: <https://ieeexplore.ieee.org/document/6638896>.
- [26] F. Fohlmeister, "GNSS Carrier Phase Tracking under Ionospheric Scintillations", thesis, Technische Universität München, 2021-04, 118 pp. Accessed: 2023-02-28. [Online]. Available: <https://elib.dlr.de/185344/>.
- [27] F. Fohlmeister, F. Antreich, and J. A. Nossek, "Dual Kalman filtering based GNSS phase tracking for scintillation mitigation", in *2018 IEEE/ION Position, Location and Navigation Symposium (PLANS)*, 2018-04, pp. 1151–1158. DOI: [10.1109/PLANS.2018.8373499](https://doi.org/10.1109/PLANS.2018.8373499).
- [28] T. E. Humphreys, M. L. Psiaki, J. C. Hinks, B. O'Hanlon, and P. M. Kintner, "Simulating Ionosphere-Induced Scintillation for Testing GPS Receiver Phase Tracking Loops", *IEEE Journal of Selected Topics in Signal Processing*, vol. 3, no. 4, pp. 707–715, 2009-08, ISSN: 1941-0484. DOI: [10.1109/JSTSP.2009.2024130](https://doi.org/10.1109/JSTSP.2009.2024130).
- [29] T. E. Humphreys, M. L. Psiaki, and P. M. Kintner, "Modeling the Effects of Ionospheric Scintillation on GPS Carrier Phase Tracking", *IEEE Transactions on Aerospace and Electronic Systems*, vol. 46, no. 4, pp. 1624–1637, 2010-10, ISSN: 1557-9603. DOI: [10.1109/TAES.2010.5595583](https://doi.org/10.1109/TAES.2010.5595583).
- [30] R. A. M. Lopes, F. Antreich, F. Fohlmeister, M. Kriegel, and H. K. Kuga, "Ionospheric Scintillation Mitigation With Kalman PLLs Employing Radial Basis Function Networks", *IEEE Transactions on Aerospace and Electronic Systems*, vol. 59, no. 5, pp. 6878–6893, 2023-10, ISSN: 1557-9603. DOI: [10.1109/TAES.2023.3281431](https://doi.org/10.1109/TAES.2023.3281431). Accessed: 2024-07-22. [Online]. Available: <https://ieeexplore.ieee.org/document/10138643>.